LANGMUIR

Article

pubs.acs.org/Langmuir

Curcumin Protects Membranes through a Carpet or Insertion Model Depending on Hydration

Richard J. Alsop, Alexander Dhaliwal, and Maikel C. Rheinstädter*

Department of Physics and Astronomy, McMaster University, Hamilton, Ontario L8S 4M1, Canada

Supporting Information

ABSTRACT: Curcumin is the main ingredient in turmeric, a common Indian spice. Curcumin shows a broad spectrum of effects, including anti-Alzheimer's and antioxidant properties. An interaction between curcumin and lipid membranes has been speculated as the root cause of this activity, and the molecule is often proposed to protect the bilayer. However, the detailed molecular mechanism of this protection is disputed. There is evidence that curcumin either (a) lies flat on the bilayer and provides a "carpet" for protection by forming a steric barrier, or (b) inserts into the membrane and stiffens tails, thereby protecting against peptide insertion. We studied the interaction between curcumin and 1,2-dimyristoyl-*sn*-glycero-3-phosphocholine (DMPC) bilayers at different concentrations using high-resolution X-ray diffraction and molecular dynamics (MD) computer simulations. We observed curcumin molecules forming a carpet in dehydrated bilayers, whereas in hydrated membranes the curcumin molecules were found to insert into the bilayers. From calculations of the potential of mean force (PMF), we find two minima, a metastable state in the headgroup region, at $|z| \approx 22$ Å, and a global minimum in the hydrophobic membrane core, at $|z| \approx 9$ Å. The population of the two states depends on membrane hydration. Experiments may thus observe curcumin in a carpet or inserted position, depending on the osmotic pressure conditions created, for instance, by salts, buffer solutions, substrates, or macromolecular solutes. In the carpet model, curcumin dehydrates lipid bilayers and decreases fluidity. When inserted, curcumin leads to a further fluidification of the membranes and an increase in tail fluctuations, contrary to cholesterol's condensing effect.

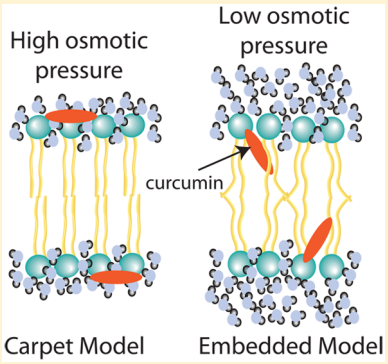

1. INTRODUCTION

Curcumin is the active ingredient in the Indian spice, turmeric. In addition to being a food additive and preservative, it is used as an anti-inflammatory agent in traditional Chinese and Indian medicine. More recently, there is evidence for curcumin as an anti-Alzheimer's, antioxidant, anticancer, and anti-inflammatory agent.[1−3]

There is intense interest in identifying the general mechanism of curcumin. Curcumin seems to influence a number of structurally unrelated proteins and processes. For example, there is evidence that curcumin affects the cross-β structure of aggregated amyloid-β peptides,[3] inhibits the formation of amyloid-β oligomers, and binds to plaques.[4] It also reduces lipid peroxidation by oxidizing Fe^{3+} free radicals.[2] The breadth of curcumin's interactions has led to speculation that it may alter the membrane environment and indirectly lead to the observed effects.[5]

Curcumin is a very hydrophobic molecule (Figure 1a) and has indeed been observed to partition into lipid membranes. The molecule was reported to cause membrane thinning, influence the bilayer's mechanical properties, and change lipid domain behavior.[5−7] Curcumin partitioning was found to stiffen the membrane, which indirectly influences the diffusion of the epidermal growth factor receptor, affecting protein behavior and potentially revealing anticancer properties.[8] A novel mechanism for the antioxidant properties of curcumin (and other flavenoids) was proposed whereby curcumin stiffens the membrane and slows lipid and ion diffusion, thereby decreasing oxidation rates.[9] Curcumin was also shown to protect the membrane against disruption by Aβ by acting as a physical barrier and preventing the insertion of the peptide.[10,11]

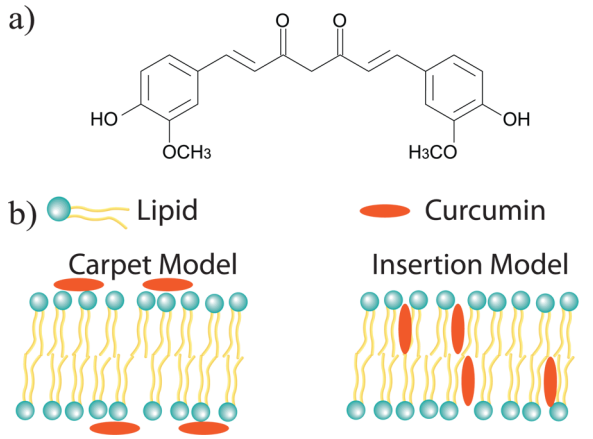

Figure 1. (a) Curcumin molecule. (b) Cartoons of the two models proposed to explain curcumin's protective membrane effects: the carpet and insertion models.

Received: May 9, 2017
Revised: May 25, 2017
Published: May 26, 2017

DOI: 10.1021/acs.langmuir.7b01562
Langmuir XXXX, XXX, XXX−XXX

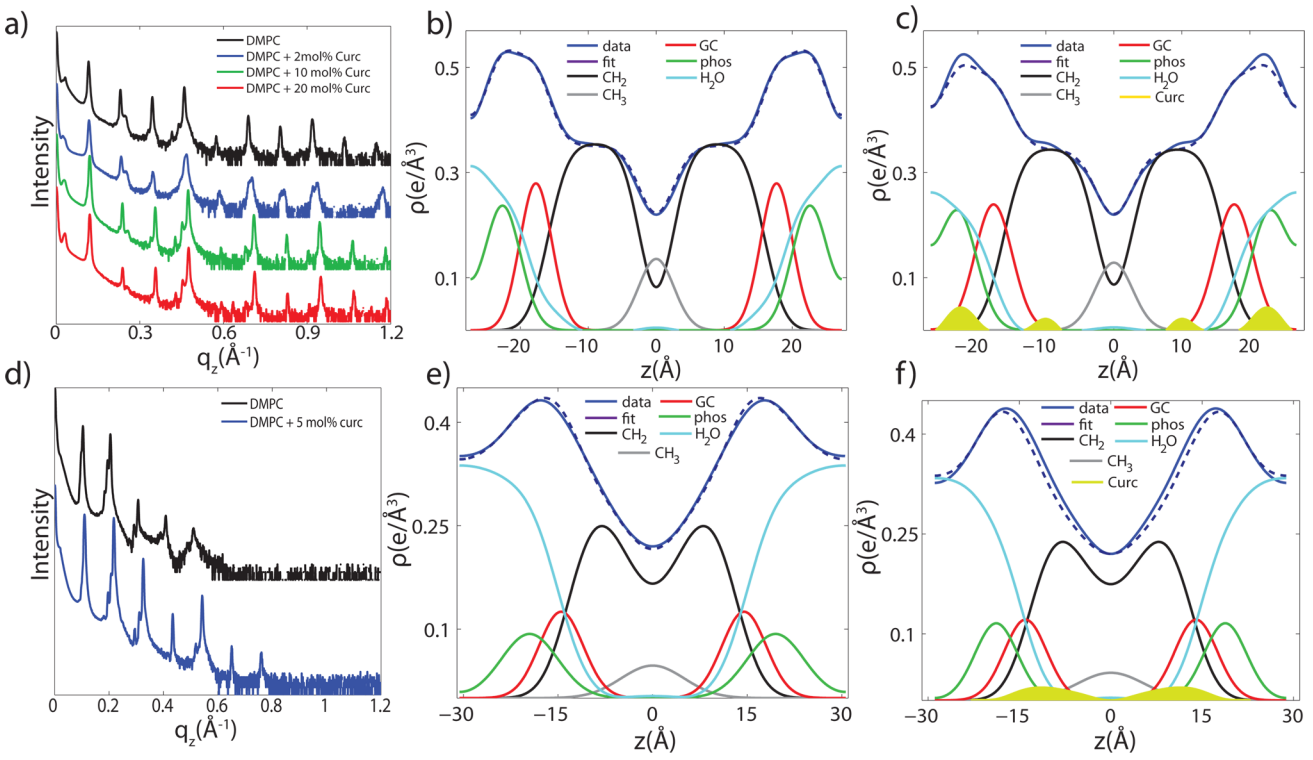

Figure 2. X-ray diffraction of dehydrated membranes with curcumin. (a) Out-of-plane diffraction. (b) Pure DMPC bilayer fit with a component group model. (c) DMPC + 2 mol % curcumin fit with a component group model. The highlighted areas indicate the residual density associated with the curcumin molecules. Curcumin molecules were found at $|z| \approx 21$ Å and $|z| \approx 10$ Å. Results of the X-ray experiments on fluid membranes: (d) q_z plots. (e) DMPC membranes fit to the component group model. (f) Membranes + 5 mol % curcumin fit to the component group model. The highlighted residual density at $|z| \approx 8$ Å was assigned to curcumin molecules.

Two models have been proposed to explain how curcumin protects lipid membranes on a molecular level. Some results suggest that curcumin lies flat on the lipid headgroups, where it forms hydrogen bonds with the lipid molecules. In this position, curcumin can act as a physical barrier, a so-called carpet, preventing peptide or oxidant penetration.[6,8,12] In contrast, curcumin can also embed deeply into the membrane and intercalate with the lipid tails.[5,9,13−15] Similar to cholesterol, in this position curcumin is proposed to increase the lipid chain order and stiffen membranes, thereby slowing lipid kinetics and increasing the energy barrier to ion or peptide embedding. The two models are pictured in Figure 1b.

In this study, we investigated the interaction between curcumin and lipid bilayers using high-resolution X-ray diffraction and molecular dynamics (MD) computer simulations at different levels of membrane hydration to mimic different osmotic pressure conditions. In the experiments, we used a novel assay of synthetic oriented lipid bilayers that has become relevant for measuring drug−membrane and peptide−membrane interactions on the nanometer scale.[16−24] In experiments and simulations, curcumin was found in both of its suggested locations, and the population of the two states was found to be dependent on membrane hydration.

2. RESULTS

Highly oriented multilamellar membrane stacks of fully saturated 1,2-dimyristoyl-*sn*-glycero-3-phosphocholine (DMPC) were prepared for the X-ray diffraction experiments, and similar systems were constructed for MD simulations such that the results between experiments and simulations can be compared. Details are provided in the Materials and Methods section. All membranes were scanned at a temperature of T = 28 °C. Fluid membranes were simulated at T = 28 °C, and 17 °C was required for the gel-phase simulations. Curcumin was added to the membranes at concentrations between 0 and 20 mol %. To investigate the role of membrane hydration, two sets of membranes were constructed in experiments and simulations: dehydrated bilayers with ∼7 hydration water molecules per lipid molecule, and fully hydrated bilayers with ∼27 water molecules per lipid. In the experiment, membrane stacks were exposed to 50% and 100% relative humidity in order to achieve the two different hydration states.

2.1. X-ray Diffraction Experiments. *2.1.1. Dehydrated Membranes.* Out-of-plane diffraction data for a pure DMPC membrane and curcumin concentrations of 2, 10, and 20 mol % is shown in Figure 2a. Ten well-developed and equally spaced Bragg peaks were observed, indicating well-ordered lamellar structures. The lamellar spacing of the bilayers, d_z, is calculated using $d_z = 2\pi/\Delta q_z$. d_z for a pure DMPC membrane was determined to be 54.7 Å, in good agreement with previous reports on DMPC at low hydration.[26,27]

Membranes with curcumin also formed well-ordered lamellar membrane stacks. However, the lamellar spacing monotonically decreased with increasing curcumin concentration to 52.8 Å at 20 mol % curcumin. This is in agreement with Hung et al., who reported a decrease in lamellar width with curcumin[7] from X-ray diffraction of multilamellar vesicles.

To determine the position of curcumin in the bilayer and to model changes to the atomic-level bilayer structure, electron density profiles were constructed for the pure DMPC membranes, as well as for membranes with 2 mol % curcumin. $\rho(z)$ for the pure DMPC membrane is shown in Figure 2b. The

DOI: 10.1021/acs.langmuir.7b01562
Langmuir XXXX, XXX, XXX−XXX

maximum in the electron density at $|z| \approx 20$ Å represents the position of the electron-rich headgroups. The bilayer density decreases to a minimum in the center of the bilayer at $z = 0$, between the tails, where CH_3 groups reside. The distance between the maxima is assigned to the bilayer head-to-head spacing, d_{HH}, and the thickness of the water layer was determined using $d_w = d_z - d_{HH}$. d_{HH} was determined to be 41 Å and slightly increased at 20 mol % curcumin to 42.8 Å. At the same time, the water layer was found to decrease significantly in width from $d_w = 13.2$ Å for DMPC to $d_w = 10.0$ Å. Values for d_{HH} and d_z for all membranes are given in Table 1. The area per lipid, A_L, was determined from in-plane diffraction (complete two-dimensional data are shown in Figure S1 in the Supporting Information).

Table 1. Structural Parameters from X-ray Diffraction and MD Simulations[a]

curcumin (mol %)	n_w	A_L (Å^2)	d_z (Å)	d_{HH}(Å)	d_w(Å)
X-ray Diffraction					
0	7	40.6	54.6	41.4	13.2
2	5.2	40.6	53.9	41.5	12.4
10		40.6	53.1	42.7	10.4
20		41.1	52.8	42.8	10.0
0	25.6	59.9[b]	61.2	35.8	25.4
5	23.0	59.9[b]	57.8	34.8	23
MD Simulations					
0	7	49	51	39	12
2	5.2	48.4	51.4	39	12
0	27	59.5	58.7	32.4	26.3
2	25	60.8	58.6	32.2	26.4

[a]Membranes were studied in a dry (~7 hydration water molecules at 50% RH) and a hydrated, fluid state (~27 hydration water molecules at 100% RH). The lamellar spacing, d_z, membrane thickness, d_{HH}, and hydration water layer thickness, d_w, were determined from out-of-plane diffraction and electron density calculations. The area per lipid (A_L) was experimentally determined for dry membranes only. [b]Fluid areas were taken from ref 25.

A component group model was fit to the electron densities.[26,28] The model decomposes the bilayer into five components: the CH_3 groups in the center of the bilayer ($\rho_{CH_3}(z)$); a function for the methylene tails in each leaflet ($\rho_{CH_2}(z)$); a profile for the glycerol chemical group in the heads ($\rho_{GC}(z)$); a profile for the phosphate group ($\rho_P(z)$); and a profile for the combined water and choline group ($\rho_{BC}(z)$). The results for DMPC (shown in Figure 2b) agree well with past observations.[26,28] All fitting parameters are given in Table 2.

The component group analysis was then applied to the electron density of DMPC +2 mol % curcumin in Figure 2c. In the fitting process, the width of the individual component groups was fixed to the values determined from pure DMPC. The positions of the groups, z_P, z_{GC}, and d_c, were adjusted to accommodate the d_{HH} observed in the experimental density. The model assumes that the structure of the bilayer is not altered significantly by 2 mol % curcumin such that excess electron density can be attributed to the presence of curcumin in the bilayers. This analysis suggests multiple binding sites for curcumin in the dehydrated bilayers: at $|z| \approx 21$ Å in the lipid headgroups and at $|z| \approx 10$ Å in the hydrophobic membrane core. From the integrated intensities, the population of the headgroup state is estimated to be 2.5:1 vs the tail group state.

2.1.2. Hydrated Membranes. Out-of-plane scans for pure DMPC membranes and membranes with 5 mol % curcumin measured at 100% RH are shown in Figure 2d. The out-of-plane scattering for the hydrated DMPC membranes produced only 5 Bragg peaks as compared to 10 in the dehydrated state. The absence of higher-order Bragg peaks and a lamellar spacing of $d_z = 61.3$ Å are consistent with a highly fluid structure.[29]

Electron density profiles were generated (Figure 2e,f), and the component group model was applied. The different groups become considerably broader in fluid membranes. Fitted parameters are given in Table 2, and structural parameters are given in Table 1. The excess electron density in Figure 2f suggests that in fluid bilayers the curcumin molecules reside entirely in the membrane tailgroup region, with an average position of $|z| \approx 8$ Å.

2.2. Molecular Dynamic Simulations. *2.2.1. Dehydrated Membranes.* United-atom MD simulations were performed with curcumin in a 128-lipid DMPC membrane. Simulations were performed with 7 water molecules per lipid molecule in order to mimic experimental conditions. To create a bilayer in the gel phase, the carbon bonds along the lipid chains were forced into an all-trans configuration for 100 ns. Next, the bonds were released and the system was simulated for 200 ns. After this procedure, the system equilibrated with $A_L = 49$ Å^2 and $d_z = 51$ Å. The temperature was kept at 17 °C; higher

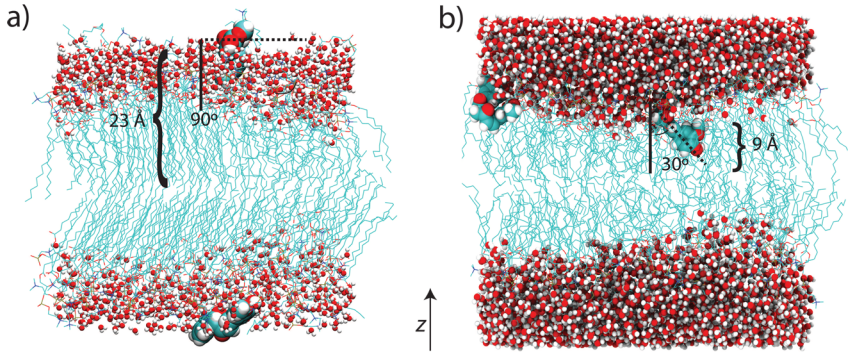

Figure 3. (a) In simulations of dehydrated membranes, curcumin was found to lie flat on the bilayer surface (90°) at $|z| \approx 23$ Å and hydrogen bond with the lipid headgroups, compatible with the carpet model. Experiments and PMF calculations show a second embedded state of the molecule at $|z| \approx 9$ Å that was not populated on the time scales of the simulations. (b) In hydrated bilayers, the curcumin molecule was found to embed within the tails at $|z| \approx 9$ Å at a tilted angle compatible with the insertion model. Molecules were fluctuating between 20 and 90° with an average tilt angle of 65° (~30° in this snapshot).

DOI: 10.1021/acs.langmuir.7b01562
Langmuir XXXX, XXX, XXX−XXX

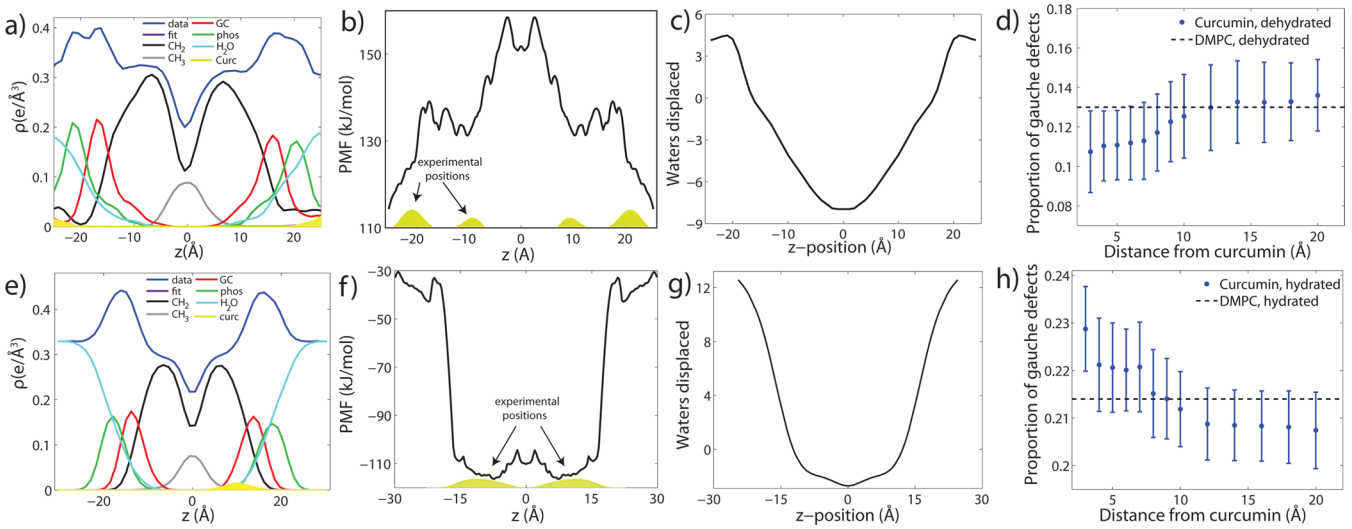

Figure 4. Analysis of the MD simulations in the dry (a–d) and hydrated (e–g) membranes. (a) A component group density model, showing the position of the curcumin densities in the dehydrated membrane. (b) Results of the umbrella simulations: the potential of mean force (PMF) for the curcumin in each umbrella window. (c) Number of water molecules displaced from a 5 Å radius around a curcumin molecule, calculated at each umbrella window and smoothed by 1 Å. (e) Component group density model showing the curcumin density in the fluid membrane. (f) PMF for curcumin in the hydrated bilayer. Experimentally determined positions are marked for comparison. (g) The number of water molecules displaced from a 5 Å radius around a curcumin molecule, in a hydrated membrane. (d) Proportion of gauche defects as a function of distance from the curcumin molecule, compared to pure DMPC. (h) Gauche defects for the hydrated membrane.

temperatures caused the system to transition into a fluid state in the simulations. Two curcumin molecules were introduced into the pure bilayer system and simulated for another 200 ns, corresponding to ∼2 mol %. A snapshot is shown in Figure 3a. The curcumin molecules were initially placed at the edge of the thin water layer and spontaneously entered the headgroups within ∼10 ns.

The final 50 ns of each simulation was used for the analysis. Electron density profiles of the various system components were generated via number density calculations along the z coordinate and scaled using the appropriate weighting based on the number of electrons within each component. The component analysis is shown in Figure 4a. The yellow areas highlight the positions of the curcumin molecules in the region of the phosphate group at $z \approx 23$ Å, in good agreement with the experiments. At this position, each curcumin molecule forms multiple hydrogen bonds with the lipid headgroups. The dehydrated bilayers equilibrated to an area per lipid of 48.4 Å^2 and d_z = 51.4 Å. The structural parameters for all simulations are summarized in Table 1.

Umbrella simulations were performed to calculate the potential of mean force (PMF). The results are displayed in Figure 4b. The PMF reveals a local minimum at $|z| \approx 9$ Å, but the absolute minimum in the profile occurs at the edge of the bilayer system. These two states agree well with the observed positions of curcumin in the X-ray experiments. We did not observe a curcumin molecule in the 9 Å position in the simulations, likely because the insertion process takes significantly longer than 200 ns.

In addition to the PMF, in every umbrella window, the change in the number of water molecules per lipid near a curcumin molecule was calculated. The number of water molecules per lipid in a radius of 5 Å around the curcumin molecule was calculated and compared to the value of the bulk membrane. As shown in Figure 4c, when the curcumin molecule is fixed in the water layer or the headgroups, there is a decrease in the number of water molecules in the surrounding area.

2.2.2. Hydrated Membranes. Membrane simulations were performed with curcumin in fully hydrated bilayers at 28 °C for 27 water molecules per lipid molecule. Two curcumin molecules were introduced and found to partition spontaneously into the tailgroup region within 50 ns. The system was simulated for 200 ns. A snapshot is shown in Figure 3b. An area per lipid of 61 Å^2 was achieved with d_z = 60.5 Å, in good agreement with the experimental value for d_z, the fully hydrated area of 60.8 Å^2 reported for the GROMOS54a7 force field,[30] and the experimentally determined value of 59.9 Å^2[25] (both determined at 30 °C).

The component analysis is shown in Figure 4e and demonstrates that the curcumin molecules partition deeply into the tail region, at $z \approx 10$ Å, in agreement with previous reports[13] and our experimental findings. At this position, each curcumin molecule still participates in hydrogen bonding with the lipid headgroups, forming one bond each. The tilt of the curcumin was also measured as the angle between the long axis of the molecule projected on the z axis of the bilayer. The tilt was measured every 1 ns and averaged over the final 50 ns. Although the tilt is a dynamic quantity that fluctuated between 20 and 90°, the curcumin molecules were on average tilted by ∼65°.

The results from umbrella simulations are displayed in Figure 4f. The minima in the PMF at $|z|$ = 9 Å are in excellent agreement with the simulated densities and the experimental results. The number of water molecules per lipid in an area of 5 Å around the curcumin molecule is shown in Figure 4g. Following that, curcumin increases the number of water molecules in the membranes when inserted.

In addition to structural parameters, the number of gauche defects in the lipid tails, i.e., kinks in the lipid alkyl chains, was calculated as a function of the lateral distance from the curcumin molecules. This quantity is often used as a direct measure of fluidity.[31−33] The proportion of gauche dihedrals

DOI: 10.1021/acs.langmuir.7b01562
Langmuir XXXX, XXX, XXX−XXX

was analyzed using a dynamic selection of lipid molecules located within a specified radius around the curcumin molecules. The results are shown in Figure 4d,h. There was a decrease in the proportion of gauche defects near curcumin in the gel phase, and an increase in the fluid phase.

3. DISCUSSION

Different models for where curcumin embeds in the membranes propose different mechanisms for its supposed protective effects. The carpet model suggests that curcumin lies flat on lipid heads and provides a steric barrier against molecular binding. Models that suggest curcumin embeds in the membrane core propose that curcumin has a mechanism similar to cholesterol: by increasing the lipid chain order, the molecule stiffens tails and increases energy barriers against insertion.

Care was taken to prepare comparable systems for experiments and simulations, and there is a strong agreement of the structural properties between the experimental and simulated systems. In fully hydrated bilayers, differences between experimental and simulated curcumin positions can be the result of bilayer undulations present in the bilayer stacks that are not accurately replicated using the short time scale and small patch size of the simulations. The undulation fluctuations in membranes were previously measured using the neutron spin−echo technique.[34,35] The corresponding undulation amplitudes can be estimated from the underlying theory of a solid supported stack of membranes by Romanov and Ul'yanov[36] to about 3 Å, which account for the observed deviations between experiments and simulations. A similar effect has been observed when comparing the diffraction experiment and MD simulations in the case of the interaction between cortisone and membranes.[23]

In dehydrated lipid membranes, the curcumin molecule was found to reside in the headgroup region, at $|z| \approx 22$ Å (21 Å in the experiment, 23 Å in the simulation). At these locations, the molecule interacts with the carbonyl moieties in the heads as well as the hydrophobic tails. The curcumin molecule lies flat on the bilayer and quickly forms hydrogen bonds with the lipid headgroups, in good agreement with the proposed carpet model.[6,8,12] A small population of curcumin molecules was found to embed at $|z| \approx 10$ Å in the experiments.

Simulation and experiment also agree that in fully hydrated bilayers, curcumin prefers to embed deeper into the membrane, at $|z| \approx 9$ Å (8 Å in experiment, 10 Å in the simulation). Simulations indicate that in this position curcumin is still forming hydrogen bonds with the headgroups. The long axis of curcumin is tilted to an average angle of ∼65° with respect to the membrane normal. This is in contrast to studies that suggest that curcumin positions upright with the bilayer when embedding in the tails,[3,9,13−15] similar to cholesterol.

The MD simulations give insight into the corresponding energy landscape. According to the PMF calculations, curcumin has two preferred locations in lipid bilayers. The position in the headgroup region was found to be metastable in both hydrated and dehydrated bilayers. Locating into the lipid tail region becomes more favorable with increasing hydration of the membranes.

We note that to achieve low hydration in our experiments and simulations, water must be removed and the reduced hydration water layer thickness may increase interbilayer interactions given the periodicity of both systems. The increased headgroup−headgroup interaction may have the potential to influence the position of curcumin by increasing the potential for hydrogen bonding. However, on the basis of the PMF in Figure 4c, the embedded state is significantly less favorable than in hydrated bilayers, suggesting that headgroup interactions due to periodicity likely do not influence the result.

In experiments presented here, reduced membrane hydration was achieved through exposure of the membranes to reduced relative humidity. A relative humidity of p/p_0 creates an osmotic pressure of $\Pi_{osm} = (k_B T/v_w) \ln(p_0/p)$, where v_w is the partial molar volume of a water molecule.[37] In membranes, this osmotic pressure leads to an attractive potential that is proportional to the thickness of the hydration water later, $V(d_w) = \Pi_{osm}\, d_w$. Membrane swelling, i.e., the absorption of hydration water molecules from the surrounding water vapor, is the result of water molecules migrating into the membrane stack, leading to an increase in the hydration water layer thickness against the attractive forces between neighboring bilayers in the stack. As the chemical potential of water molecules in relative humidity is reduced by $\Delta\mu_w = k_B T \ln(p/p_0)$, this process can be inhibited at reduced humidity levels.

Changes in osmotic pressure can directly be related to the swelling of the membranes and the thickness of the hydration water layer in the experimental system. Petrache et al.[38] and Mennicke, Constantin, and Salditt[39] measured the lamellar spacing of DMPC bilayers for different osmotic pressures by varying the concentration of poly(ethylene glycol) (PEG). A d_z spacing of 53 Å, for instance, was observed at an osmotic presssure of $\Pi \approx 7 \times 10^6$ Pa. Protein solutions can also cause osmotic stress,[40] depending on their concentration. The osmotic pressure of a physiological saline solution with a density of 1.005 g/mol at 37 °C is calculated to be 760 000 Pa. The osmotic pressure of a typically used 10 mM Hepes buffer solution corresponds to ∼26 000 Pa. The physiological saline and Hepes buffer solutions would thus reduce the lamellar d_z-spacing in DMPC from 61 Å to ∼53 Å, respective, ∼59 Å. By using swelling data from the Nagle group,[29] these d_z spacings correspond to relative humidity levels of ∼99% and close to 100%. The relation among osmotic pressure, relative humidity, and lamellar spacing is plotted in Figure 5.

These results can help to unify the different models that have been suggested for curcumin's position and effects. In different

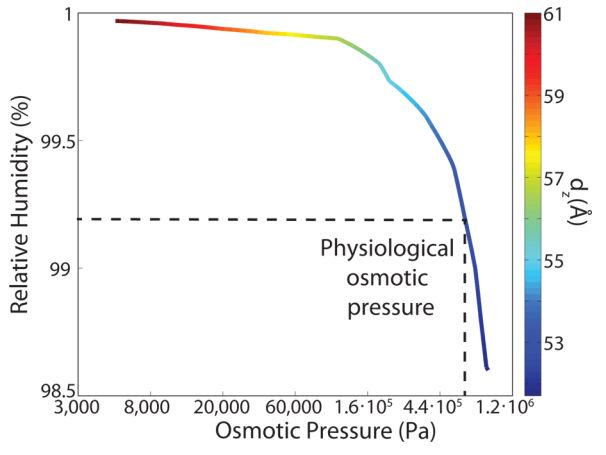

Figure 5. Relation among the osmotic pressure, relative humidity, RH, and lamellar spacing, d_z, of DMPC bilayers. Data for bilayer swelling as a function of RH were taken from Chu et al.[29] d_z as a function of osmotic pressure was determined by Petrache et al.[38] and Mennicke, Constantin, and Salditt.[39]

DOI: 10.1021/acs.langmuir.7b01562
Langmuir XXXX, XXX, XXX−XXX

biological environments, such as salts and buffer solutions, the presence of substrates or macromolecular solutes may lead to an effective dehydration of lipid bilayers, and it is plausible that they can shift the population of the two preferred curcumin locations in the membranes. Some experiments may thus observe curcumin in carpet or inserted depending on the experimental conditions. Curcumin's effect on lipid membranes strongly depends on its location.

In the carpet model, the presence of curcumin molecules in the lipid headgroups led to a decrease in the fluidity and dehydration of the bilayers, as reported previously. We do not find evidence for a cholesterol-like chain ordering effect of curcumin in the insertion model. For one, the molecule does not insert into our bilayers with an upright orientation. Second, d_{HH} does not increase when curcumin is added to fluid-phase bilayers but in fact slightly decreases, by ∼1 Å in experiments and by 0.2 Å in simulations. The protective effect of curcumin in the insertion model is thus not similar to cholesterol's stiffening and condensation effect. Instead, curcumin was found to increase the number of water molecules in the bilayers and the number of gauche defects, making the bilayers more fluid. This finding is inconsistent with the current literature hypothesis, as described in the Introduction, which involves curcumin increasing the lipid chain order similarly to cholesterol. Future work including curcumin and peptides is needed to unveil the exact mechanism of how curcumin can inhibit peptide insertion in the insertion model under these circumstances.

4. CONCLUSIONS

Curcumin was added to phospholipid bilayers made of DMPC, and partitioning of the molecule was studied using high-resolution X-ray diffraction and MD simulations. Curcumin was found in two locations in the membranes: in the lipid headgroups at z values of $|z| \approx 22$ Å lying flat on the bilayer edge and inside the hydrophobic membrane core, tilted with respect to the bilayer normal, at $|z| \approx 9$ Å. The population of the two states was found to depend on membrane hydration. While the headgroup position is metastable, the core position becomes significantly more favorable with increasing hydration.

The two observed positions correspond to the two models for curcumin's protective properties: in the carpet model, it lies flat on the bilayer and provides a carpet for protection by forming a steric barrier, whereas in the insertion model, it protects against peptide insertion. We suggest that curcumin can be observed in carpet or inserted depending on the osmotic pressure conditions created by salts, buffer solutions, substrates, or macromolecular solutes.

It was suggested that curcumin stiffens membranes and decreases lipid diffusion and increases the energy barrier to molecule binding, similar to the effect of cholesterol. In the carpet model, the presence of curcumin molecules in the lipid headgroups led to a decrease in fluidity and the dehydration of the bilayers. With the insertion models, we find that curcumin leads to a further fluidification of lipid membranes at high hydration levels, in contradiction to cholesterol's condensing effect.

5. MATERIALS AND METHODS

5.1. Preparation of the Highly Oriented Multilamellar Membrane Complexes. Highly oriented multilamellar membranes were prepared on polished 1×1 cm^2 silicon wafers. The wafers were first pretreated by sonication in dichloromethane (DCM) at 310 K for 25 min to remove all organic contamination and create a hydrophobic substrate. After removal from DCM postsonication, each wafer was thoroughly rinsed three times by alternating with ∼50 mL of ultrapure water (18.2 MΩ·cm) and methanol. This treatment renders the surface of the wafers hydrophobic.

Table 2. Fitting Parameters of the Component Group Analysis

curcumin (mol %)	n_w	σ_{CH_3} (Å)	σ_{CH_2} (Å)	d_c (Å)	σ_{GC} (Å)	z_{GC} (Å)	σ_p (Å)	z_p (Å)
0	7	2.6	2.4	15.9	2.4	17.6	2.65	22.6
2	5.2	2.7	2.4	16.2	2.4	17.9	2.65	22.95
0	27.6	5	3.5	13	3.6	14.5	3.5	18.5
5	25.0	5	3.5	13	3.5	14	3.5	18.5

1,2-Dimysteroyl-*sn*-glycero-3-phosphocholine (DMPC) is initially dissolved in a chloroform solution. Curcumin (Sigma, SAS 458-37-7) is also dissolved in chloroform and then mixed with the lipid solution. The chloroform was then evaporated, and the lipid-curcumin precipitate was redissolved in either pure water or a 1:1 solution of trifluoroethanol and chloroform. Water solutions were point sonicated, and TFE/chloroform solution was vortex mixed and heated to 313 K.

A tilting incubator was heated to 313 K, and the solutions were placed inside to equilibrate. A lipid solution (80 μL) was deposited on each wafer. The solvent was then allowed to slowly evaporate while being gently rocked such that the lipid solution spread evenly on the wafers. Samples were then placed in a sealed container containing an open vial of ultrapure water and incubated for 24 h at 100% RH at 303 K. This procedure results in highly oriented multilamellar membrane stacks and a uniform coverage of the silicon wafers. About 3000 highly oriented stacked membranes with a total thickness of ∼10 μm are produced using this protocol.

5.2. X-ray Diffraction Experiment and Construction of Electron Densities. Out-of-plane X-ray diffraction measurements were obtained using the Biological Large Angle Diffraction Experiment (BLADE) in the Laboratory for Membrane and Protein Dynamics at McMaster University. BLADE uses a 9 kW (45 kV, 200 mA) Cu Kα Rigaku Smartlab rotating anode at a wavelength of 1.5418 Å. Both the source and detector are mounted on moveable arms such that the membranes stay horizontal during measurements. Focusing multilayer optics provide a high-intensity parallel beam with monochromatic X-ray intensities of up to 10^{10} counts/(s × mm^2). This beam geometry provides optimal illumination of the membrane samples to maximize the scattered signal. By using highly oriented stacks, the out-of-plane (q_z) structure of the membranes could be determined independently from the in-plane ($q_\parallel$) structure.

Electron densities, $\rho(z)$, were calculated through Fourier transform of the integrated intensities of the reflectivity Bragg peaks. $\rho(z)$ can be approximated by one-dimensional Fourier analysis

$$\rho(z) = \frac{2}{d_z} \sum_{n=1}^{N} \sqrt{I_n q_n}\, \nu_n \cos\left(\frac{2\pi n z}{d_z}\right) \quad (1)$$

where N is the highest order of the Bragg peaks observed in the experiment. The integrated reflectivity Bragg peak intensities, I_n, are multiplied by q_n to generate form factors $F(q_n)$. The bilayer form factor, which is in general a complex quantity, is real-valued when the structure is centrosymmetric. The phase problem of crystallography therefore simplifies to the sign problem $F(q_z) = \pm|F(q_z)|$, and the phases, ν_n, can take only values of ±1.

The phases, ν_n, were assessed by fitting the experimental peak intensities, as detailed in Figure S1 in the Supporting Information. To transform the $\rho(z)$ to an absolute scale, the curves were vertically shifted to fulfill the condition $\rho(0) = 0.22e^-/Å^3$ (the electron density of a CH_3 group) in the center of a bilayer. The curves were then scaled until the total number of electrons $e^- = A_L \int_0^{dz/2} \rho(z)\, dz$ across a membrane leaflet agrees with the total number of electrons of a

DOI: 10.1021/acs.langmuir.7b01562
Langmuir XXXX, XXX, XXX−XXX

DMPC molecule with n_w water molecules and the contribution from curcumin.

To determine the number of water molecules per lipid, n_w, the following relation was used

$$\frac{1}{2}A_L d_z = V_L + n_w V_w \quad (2)$$

where A_L is the area per lipid, V_L is the volume per lipid, and V_w is the volume per water molecule, known to be 30 Å^3. For DMPC in the gel phase at low hydration, the volume per lipid was calculated previously to be V_L = 891 Å^3,[26] whereas the fluid volume of V_L = 1101 Å^3 was taken from ref 41. We note that V_L for the dehydrated gel phase is lower than the value of 1041 Å^3 reported by Tristram-Nagle et al. for hydrated gel membranes.[27] The discrepancy is mainly the effect of reduced hydration resulting in a reduced area per lipid, A_L. We measure $A_L \approx 41$ Å^2 to be in good agreement with previous reports for dehydrated gel phases,[42,43] and Tristram-Nagle et al. report 47 Å^2 in the hydrated gel phase.

5.3. Real-Space Modeling of Electron Density Profiles. To model the bilayer structure and determine the position of the curcumin molecule, electron density profiles were decomposed using a composite model. The specific models used for the lipid component groups are those used by Klauda et al. and Alsop et al.[28] Atoms from the DMPC molecules were distributed between five component groups representing distinct portions of the bilayer. These regions are (1) the terminal CH_3 groups at the end of the lipid chains, for both lipids in the bilayer, found in the center of the bilayer (CH_3); (2) the CH_2 groups composing the hydrocarbon core of the lipid molecule (CH_2); (3) the glycerol moiety in the headgroup (GC); and (4) the phosphate group in the headgroup (P). An additional function is added to describe the hydration water layer and the choline group of the lipid (BC). The functions describe a full bilayer, i.e., two leaflets. For a detailed description of the model, please see refs 26 and 28.

In total, there are seven to nine free parameters in the fitting: the width of the CH_3 peak, σ_{CH_3}, the width of the tail CH_2 interface, σ_{CH_2}, the thickness of the hydrocarbon region, d_C; and the positions and widths of the glycerol and phosphate groups, z_{GC}, σ_{GC}, z_P, and σ_P. Because the phosphate and glycerol groups are coupled by chemical bonds, σ_{GC}, σ_p, and σ_{CH_2} are softly constrained to covary.

To determine the position of the curcumin molecule, the component group model is first applied to the pure DMPC membrane in the appropriate hydration state. Next, the same fitting parameters are applied to the electron density for membranes with curcumin. Adjustments are made to z_p, z_{GC}, and d_c so that the fitting to d_{HH} matches the experimental value. The density that remains after the lipids are subtracted from the measured density is attributed to the curcumin molecule.

5.4. Molecular Dynamics Simulations. All simulations were run in-house on MacSim, a GPU accelerated workstation with 20 physical Intel XeonCPU cores and 2 GeForce GTX 1080 high-power graphics cards resulting in 5120 CUDA Cores. This system produces about 180 ns of MD simulations in standard 128 lipid membrane patches in GROMACS.

A system of 128 DMPC lipids (64 per leaflet) was taken from Tieleman et al.[44] and re-equilibrated for 500 ns. Curcumin topology was obtained using the Automated Force Field Topology Builder (ATB).[45,46] The SPC water model was used for system solvation.[47] All MD simulations were performed using the GROMACS 5.1.2 software package[48] implementing the GROMOS 54a7 force field[49] modified with Berger lipid parameters.[50] All simulations used a 2 fs time step, a periodic boundary condition applied to all directions, the particle-mesh Ewald method to solve for long-range electrostatics,[51] a short-range van der Waals cutoff of 1.2 nm, and the LINCS algorithm to determine bond constraints.[52] Temperature coupling was controlled using a Nose-Hoover thermostat at 28 °C (τ = 0.5 ps),[53] and pressure was kept at 1.0 bar using Parrinello−Rahman semi-isotropic weak coupling (τ = 1 ps).[54]

A total of four distinct simulations were conducted. First, two pure DMPC membranes with 7 and 27 waters per lipid were simulated for 200 ns each to mimic the dehydrated and hydrated membranes, respectively. Next, two curcumin molecules were introduced into the pure membranes, and the system was simulated for another 200 ns. All analyses were performed with the final 50 ns of the simulations using GROMACS algorithms and simple scripts.[55] The electron density profiles were calculated for different constituents of the system, similar to other studies using lipid bilayers.[22,56] The function used calculates the relative distance along the bilayer normal of each atom within the specified index group, assigns a weighting based upon the number of electrons in each atom, and delivers an electron density as averaged over the specified time range.

Umbrella simulations were also performed, with the protocol based on previous studies.[23,57,58] The initial condition was a curcumin molecule placed at the membrane edge. Umbrella simulations are obtained by pulling the molecule through the bilayer, along the z direction with a force constant of 3000 kJ/mol, and umbrella windows are obtained with Δz = 1 Å. Each window is then simulated for 15 ns. Potentials of mean force (PMFs) are then calculated using the weighted histogram analysis method in GROMACS,[59] with the final 5 ns of each umbrella window and the center of the bilayer as the reference point.

The proportion of gauche dihedrals within a lipid system is commonly used as a measure of bilayer fluidity.[31−33] The proportion of gauche dihedrals as a function of increasing distance from curcumin was determined using dynamic scripting and GROMACS algorithms. A script was constructed to generate an index file containing only carbon chains belonging to lipids within the specified radius from the center of mass of any curcumin molecule within the system every 50 frames. This index file specified the DMPC molecules whose carbons were to be used in the calculation of the Ryckaert−Bellemans dihedral angles over that time interval.[60] This was repeated over the final 50 ns of the simulation and averaged for each carbon position. Averaging across the SN1 and SN2 tails was then performed to generate the value shown in Figure 4d,h, and the script was run successively to consider each new distance from curcumin. Testing with the script showed that windows shorter than 50 frames did not produce statistically different results, so this frame length was used to decrease the computational time.

■ ASSOCIATED CONTENT

Supporting Information

The Supporting Information is available free of charge on the ACS Publications website at DOI: 10.1021/acs.langmuir.7b01562.

Additional analysis of X-ray diffraction data (PDF)

■ AUTHOR INFORMATION

Corresponding Author

*E-mail: rheinstadter@mcmaster.ca. Phone: +1-(905)-525-9140-23134. Fax: +1-(905)-546-1252.

ORCID

Richard J. Alsop: 0000-0003-0563-0063

Notes

The authors declare no competing financial interest.

■ ACKNOWLEDGMENTS

This research was funded by the Natural Sciences and Engineering Research Council of Canada (NSERC), the National Research Council Canada (NRC), the Canada Foundation for Innovation (CFI), and the Ontario Ministry of Economic Development and Innovation. R.J.A. is the recipient of an NSERC PGS-D scholarship. A.D. is the recipient of an NSERC USRA. M.C.R. is the recipient of an Early Researcher Award of the Province of Ontario and a University Scholar Award from McMaster University.

DOI: 10.1021/acs.langmuir.7b01562
Langmuir XXXX, XXX, XXX−XXX

REFERENCES

(1) Hu, S.; Maiti, P.; Ma, Q.; Zuo, X.; Jones, M. R.; Cole, G. M.; Frautschy, S. A. Clinical development of curcumin in neurodegenerative disease. *Expert Rev. Neurother.* **2015**, *15* (6), 629−637.

(2) Hamaguchi, T.; Ono, K.; Yamada, M. REVIEW: Curcumin and Alzheimeras disease. *CNS Neurosci. Ther.* **2010**, *16* (5), 285−297.

(3) Ak, T.; Gülçin, İ Antioxidant and radical scavenging properties of curcumin. *Chem.-Biol. Interact.* **2008**, *174* (1), 27−37.

(4) Yang, F.; Lim, G. P.; Begum, A. N.; Ubeda, O. J.; Simmons, M. R.; Ambegaokar, S. S.; Chen, P. P.; Kayed, R.; Glabe, C. G.; Frautschy, S. A.; Cole, G. M. Curcumin inhibits formation of amyloid β oligomers and fibrils, binds plaques, and reduces amyloid in vivo. *J. Biol. Chem.* **2005**, *280* (7), 5892−5901.

(5) Ingolfsson, H. I.; Koeppe, R. E.; Andersen, O. S. Curcumin is a modulator of bilayer material properties. *Biochemistry* **2007**, *46* (36), 10384−10391.

(6) Varshney, G. K.; Kintali, S. R.; Gupta, P. K.; Das, K. Effect of Bilayer Partitioning of Curcumin on the Adsorption and Transport of a Cationic Dye Across POPG Liposomes Probed by Second-Harmonic Spectroscopy. *Langmuir* **2016**, *32* (40), 10415−10421.

(7) Hung, W. C.; Chen, F. Y.; Lee, C. C.; Sun, Y.; Lee, M. T.; Huang, H. W. Membrane-thinning effect of curcumin. *Biophys. J.* **2008**, *94* (11), 4331−4338.

(8) Starok, M.; Preira, P.; Vayssade, M.; Haupt, K.; Salome, L.; Rossi, C. EGFR Inhibition by Curcumin in Cancer Cells: A Dual Mode of Action. *Biomacromolecules* **2015**, *16* (5), 1634−1642.

(9) Arora, A.; Byrem, T. M.; Nair, M. G.; Strasburg, G. M. Modulation of liposomal membrane fluidity by flavonoids and isoflavonoids. *Arch. Biochem. Biophys.* **2000**, *373* (1), 102−109.

(10) Lim, G. P.; Chu, T.; Yang, F.; Beech, W.; Frautschy, S. A.; Cole, G. M. The curry spice curcumin reduces oxidative damage and amyloid pathology in an Alzheimer transgenic mouse. *J. Neurosci.* **2001**, *21* (21), 8370−8377.

(11) Mishra, S.; Palanivelu, K. The effect of curcumin (turmeric) on Alzheimer's disease: An overview. *Annals of Indian Academy of Neurology* **2008**, *11* (1), 13.

(12) Thapa, A.; Vernon, B. C.; De la Peña, K.; Soliz, G.; Moreno, H. A.; López, G. P.; Chi, E. Y. Membrane-mediated neuroprotection by curcumin from amyloid-β-peptide-induced toxicity. *Langmuir* **2013**, *29* (37), 11713−11723.

(13) Kopeć, W.; Telenius, J.; Khandelia, H. Molecular dynamics simulations of the interactions of medicinal plant extracts and drugs with lipid bilayer membranes. *FEBS J.* **2013**, *280* (12), 2785−2805.

(14) Barry, J.; Fritz, M.; Brender, J. R.; Smith, P. E.; Lee, D. K.; Ramamoorthy, A. Determining the effects of lipophilic drugs on membrane structure by solid-state NMR spectroscopy: the case of the antioxidant curcumin. *J. Am. Chem. Soc.* **2009**, *131* (12), 4490−4498.

(15) Erlejman, A.; Verstraeten, S.; Fraga, C.; Oteiza, P. I. The interaction of flavonoids with membranes: potential determinant of flavonoid antioxidant effects. *Free Radical Res.* **2004**, *38* (12), 1311−1320.

(16) Balali-Mood, K.; Ashley, R. H.; Hauß, T.; Bradshaw, J. P. Neutron diffraction reveals sequence-specific membrane insertion of pre-fibrillar islet amyloid polypeptide and inhibition by rifampicin. *FEBS Lett.* **2005**, *579* (5), 1143−1148.

(17) Barrett, M. A.; Zheng, S.; Roshankar, G.; Alsop, R. J.; Belanger, R. K. R.; Huynh, C.; Kučerka, N.; Rheinstädter, M. C. Interaction of Aspirin (Acetylsalicylic Acid) with Lipid Membranes. *PLoS One* **2012**, *7* (4), e34357.

(18) Drolle, E.; Kučerka, N.; Hoopes, M.; Choi, Y.; Katsaras, J.; Karttunen, M.; Leonenko, Z. Effect of melatonin and cholesterol on the structure of DOPC and DPPC membranes. *Biochim. Biophys. Acta, Biomembr.* **2013**, *1828* (9), 2247−2254.

(19) Dies, H.; Toppozini, L.; Rheinstädter, M. C. The interaction between amyloid-β peptides and anionic lipid membranes containing cholesterol and melatonin. *PLoS One* **2014**, *9* (6), e99124.

(20) Alsop, R. J.; Barrett, M. A.; Zheng, S.; Dies, H.; Rheinstädter, M. C. Acetylsalicylic acid (ASA) increases the solubility of cholesterol when incorporated in lipid membranes. *Soft Matter* **2014**, *10* (24), 4275−4286.

(21) Tang, J.; Alsop, R. J.; Backholm, M.; Dies, H.; Shi, A. C.; Rheinstädter, M. C. Amyloid-β 25−35 peptides aggregate into cross-β sheets in unsaturated anionic lipid membranes at high peptide concentrations. *Soft Matter* **2016**, *12* (13), 3165−3176.

(22) Alsop, R. J.; Armstrong, C. L.; Maqbool, A.; Toppozini, L.; Dies, H.; Rheinstädter, M. C. Cholesterol expels ibuprofen from the hydrophobic membrane core and stabilizes lamellar phases in lipid membranes containing ibuprofen. *Soft Matter* **2015**, *11* (24), 4756−4767.

(23) Alsop, R. J.; Khondker, A.; Hub, J. S.; Rheinstädter, M. C. The Lipid Bilayer Provides a Site for Cortisone Crystallization at High Cortisone Concentrations. *Sci. Rep.* **2016**, *6*, 22425.

(24) Schmidt, A.; Löhrer, D.; Alsop, R. J.; Lenzig, P.; Oslender-Bujotzek, A.; Wirtz, M.; Rheinstädter, M. C.; Gründer, S.; Wiemuth, D. A Cytosolic Amphiphilic α-Helix Controls the Activity of the Bile Acid-sensitive Ion Channel (BASIC). *J. Biol. Chem.* **2016**, *291* (47), 24551−24565.

(25) Kučerka, N.; Nieh, M. P.; Katsaras, J. Fluid phase lipid areas and bilayer thicknesses of commonly used phosphatidylcholines as a function of temperature. *Biochim. Biophys. Acta, Biomembr.* **2011**, *1808* (11), 2761−2771.

(26) Alsop, R. J.; Schober, R. M.; Rheinstädter, M. C. Swelling of phospholipid membranes by divalent metal ions depends on the location of the ions in the bilayers. *Soft Matter* **2016**, *12* (32), 6737−6748.

(27) Tristram-Nagle, S.; Liu, Y.; Legleiter, J.; Nagle, J. F. Structure of Gel Phase DMPC Determined by X-Ray Diffraction. *Biophys. J.* **2002**, *83*, 3324−3335.

(28) Klauda, J. B.; Kučerka, N.; Brooks, B. R.; Pastor, R. W.; Nagle, J. F. Simulation-Based Methods for Interpreting X-Ray Data from Lipid Bilayers. *Biophys. J.* **2006**, *90*, 2796−2807.

(29) Chu, N.; Kučerka, N.; Liu, Y.; Tristram-Nagle, S.; Nagle, J. F. Anomalous swelling of lipid bilayer stacks is caused by softening of the bending modulus. *Phys. Rev. E* **2005**, *71* (4), 041904.

(30) Pluhackova, K.; Kirsch, S. A.; Han, J.; Sun, L.; Jiang, Z.; Unruh, T.; Böckmann, R. A. A critical comparison of biomembrane force fields: structure and dynamics of model DMPC, POPC, and POPE bilayers. *J. Phys. Chem. B* **2016**, *120* (16), 3888−3903.

(31) Saito, H.; Shinoda, W. Cholesterol effect on water permeability through DPPC and PSM lipid bilayers: a molecular dynamics study. *J. Phys. Chem. B* **2011**, *115* (51), 15241−15250.

(32) Hofsäß, C.; Lindahl, E.; Edholm, O. Molecular dynamics simulations of phospholipid bilayers with cholesterol. *Biophys. J.* **2003**, *84* (4), 2192−2206.

(33) Venable, R. M.; Brooks, B. R.; Pastor, R. W. Molecular dynamics simulations of gel (LβI) phase lipid bilayers in constant pressure and constant surface area ensembles. *J. Chem. Phys.* **2000**, *112* (10), 4822−4832.

(34) Rheinstädter, M. C.; Häußler, W.; Salditt, T. Dispersion relation of lipid membrane shape fluctuations by neutron spin-echo spectrometry. *Phys. Rev. Lett.* **2006**, *97* (4), 048103.

(35) Armstrong, C. L.; Häußler, W.; Seydel, T.; Katsaras, J.; Rheinstädter, M. C. Nanosecond lipid dynamics in membranes containing cholesterol. *Soft Matter* **2014**, *10* (15), 2600−2611.

(36) Romanov, V.; Ul'yanov, S. Dynamic and correlation properties of solid supported smectic-a films. *Phys. Rev. E: Stat. Phys., Plasmas, Fluids, Relat. Interdiscip. Top.* **2002**, *66* (6), 061701.

(37) Parsegian, V.; Rand, R. Interaction in membrane assemblies. *Handb. Biol. Phys.* **1995**, *1*, 643−690.

(38) Petrache, H. I.; Gouliaev, N.; Tristram-Nagle, S.; Zhang, R.; Suter, R. M.; Nagle, J. F. Interbilayer interactions from high-resolution x-ray scattering. *Phys. Rev. E: Stat. Phys., Plasmas, Fluids, Relat. Interdiscip. Top.* **1998**, *57* (6), 7014.

(39) Mennicke, U.; Constantin, D.; Salditt, T. Structure and interaction potentials in solid-supported lipid membranes studied by x-ray reflectivity at varied osmotic pressure. *Eur. Phys. J. E: Soft Matter Biol. Phys.* **2006**, *20* (2), 221−230.

DOI: 10.1021/acs.langmuir.7b01562
Langmuir XXXX, XXX, XXX−XXX

(40) Licata, V. J.; Allewell, N. M. [3] Measuring hydration changes of proteins in solution: applications of osmotic stress and structure-based calculations. *Methods Enzymol.* **1998**, *295*, 42−62.
(41) Nagle, J. F.; Wilkinson, D. A. Lecithin bilayers. Density measurement and molecular interactions. *Biophys. J.* **1978**, *23* (2), 159−175.
(42) Church, S.; Griffiths, D.; Lewis, R.; McElhaney, R.; Wickman, H. X-ray structure study of thermotropic phases in isoacylphosphatidylcholine multibilayers. *Biophys. J.* **1986**, *49* (3), 597−605.
(43) Raghunathan, V.; Katsaras, J. Structure of the l c? phase in a hydrated lipid multilamellar system. *Phys. Rev. Lett.* **1995**, *74* (22), 4456.
(44) Tieleman, D. P.; Sansom, M. S.; Berendsen, H. J. Alamethicin helices in a bilayer and in solution: molecular dynamics simulations. *Biophys. J.* **1999**, *76* (1), 40−49.
(45) Koziara, K. B.; Stroet, M.; Malde, A. K.; Mark, A. E. Testing and validation of the Automated Topology Builder (ATB) version 2.0: prediction of hydration free enthalpies. *J. Comput.-Aided Mol. Des.* **2014**, *28* (3), 221−233.
(46) Malde, A. K.; Zuo, L.; Breeze, M.; Stroet, M.; Poger, D.; Nair, P. C.; Oostenbrink, C.; Mark, A. E. An automated force field topology builder (ATB) and repository: version 1.0. *J. Chem. Theory Comput.* **2011**, *7* (12), 4026−4037.
(47) Berendsen, H. J.; Postma, J. P.; van Gunsteren, W. F.; Hermans, J. Interaction Models for Water in Relation to Protein Hydration. In *Intermolecular Forces: Proceedings of the Fourteenth Jerusalem Symposium on Quantum Chemistry and Biochemistry*; Pullman, B., Ed.; D. Reidel: Dordrecht, Holland, 1981; pp 331−342.
(48) Abraham, M. J.; Murtola, T.; Schulz, R.; Páll, S.; Smith, J. C.; Hess, B.; Lindahl, E. GROMACS: High performance molecular simulations through multi-level parallelism from laptops to supercomputers. *SoftwareX* **2015**, *1-2*, 19−25.
(49) Schmid, N.; Eichenberger, A. P.; Choutko, A.; Riniker, S.; Winger, M.; Mark, A. E.; van Gunsteren, W. F. Definition and testing of the GROMOS force-field versions 54A7 and 54B7. *Eur. Biophys. J.* **2011**, *40* (7), 843−856.
(50) Berger, O.; Edholm, O.; Jähnig, F. Molecular dynamics simulations of a fluid bilayer of dipalmitoylphosphatidylcholine at full hydration, constant pressure, and constant temperature. *Biophys. J.* **1997**, *72* (5), 2002.
(51) Darden, T.; York, D.; Pedersen, L. Particle mesh Ewald: An *N*log(*N*) method for Ewald sums in large systems. *J. Chem. Phys.* **1993**, *98* (12), 10089−10092.
(52) Hess, B.; Bekker, H.; Berendsen, H. J.; Fraaije, J. G. LINCS: a linear constraint solver for molecular simulations. *J. Comput. Chem.* **1997**, *18* (12), 1463−1472.
(53) Evans, D. J.; Holian, B. L. The nose−hoover thermostat. *J. Chem. Phys.* **1985**, *83* (8), 4069−4074.
(54) Parrinello, M.; Rahman, A. Polymorphic transitions in single crystals: A new molecular dynamics method. *J. Appl. Phys.* **1981**, *52* (12), 7182−7190.
(55) Van Der Spoel, D.; Lindahl, E.; Hess, B.; Groenhof, G.; Mark, A. E.; Berendsen, H. J. GROMACS: fast, flexible, and free. *J. Comput. Chem.* **2005**, *26* (16), 1701−1718.
(56) Boggara, M. B.; Krishnamoorti, R. Partitioning of nonsteroidal antiinflammatory drugs in lipid membranes: a molecular dynamics simulation study. *Biophys. J.* **2010**, *98* (4), 586−595.
(57) Wennberg, C. L.; Van Der Spoel, D.; Hub, J. S. Large influence of cholesterol on solute partitioning into lipid membranes. *J. Am. Chem. Soc.* **2012**, *134* (11), 5351−5361.
(58) Zocher, F.; Wennberg, C. L.; Pohl, P.; Hub, J. Local micropartition coefficients govern solute permeability of cholesterol-containing membranes. *Biophys. J.* **2013**, *104* (2), 82a.
(59) Hub, J. S.; De Groot, B. L.; Van Der Spoel, D. g_wham A Free Weighted Histogram Analysis Implementation Including Robust Error and Autocorrelation Estimates. *J. Chem. Theory Comput.* **2010**, *6* (12), 3713−3720.
(60) Ryckaert, J. P.; Bellemans, A. Molecular dynamics of liquid alkanes. *Faraday Discuss. Chem. Soc.* **1978**, *66*, 95−106.

DOI: 10.1021/acs.langmuir.7b01562
Langmuir XXXX, XXX, XXX−XXX